

Climate change increased heavy rainfall, hitting vulnerable communities in Eastern Northeast Brazil

Authors

Mariam Zachariah, *Grantham Institute, Imperial College London, UK*
Francisco das Chagas Vasconcelos Junior, *Ceará Institute for Meteorology and Water Resources, FUNCEME, Fortaleza, Brazil*
Thiago Luiz do Vale Silva, *Water and Climate Pernambuco Agency APAC, Recife, Brazil; and Center for Renewable Energy from the Federal University of Pernambuco CER/UFPE, Pernambuco, Brazil.*
Edvânia Pereira dos Santos, *Water and Climate Pernambuco Agency APAC, Recife, Brazil*
Caio Augusto dos Santos Coelho, *Centre for Weather Forecast and Climatic Studies, National Institute for Space Research, Brazil*
Lincoln Muniz Alves, *National Institute for Space Research (INPE), Brazil*
Eduardo Sávio Passos Rodrigues Martins, *FUNCEME, Fortaleza, Brazil*
Alexandre C. Köberle, *Grantham Institute, Imperial College London, United Kingdom*
Roop Singh, *Red Cross Red Crescent Climate Centre*
Maja Vahlberg, *Red Cross Red Crescent Climate Centre*
Victor Marchezini, *Natural Hazards Center, University of Colorado at Boulder, National Center for Monitoring and Early Warning of Natural Hazards (Cemaden)*
Dorothy Heinrich, *Red Cross Red Crescent Climate Centre*
Lisa Thalheimer, *School of Public and International Affairs, Princeton University, Princeton, USA; Potsdam Institute for Climate Impact Research, Potsdam, Germany*
Emmanuel Raju, *Department of Public Health, Global Health Section & Copenhagen Centre for Disaster Research, University of Copenhagen, Denmark*
Gerbrand Koren, *Copernicus Institute of Sustainable Development, Utrecht University, the Netherlands*
Sjoukje Philip, *Royal Netherlands Meteorological Institute (KNMI), De Bilt, The Netherlands*
Sarah Kew, *Royal Netherlands Meteorological Institute (KNMI), De Bilt, The Netherlands*
Rémy Bonnet, *Institut Pierre-Simon Laplace, CNRS, Sorbonne Université, Paris, France*
Sihan Li, *School of Geography and the Environment, University of Oxford, UK*
Wenchang Yang, *Department of Geosciences, Princeton University, Princeton, USA;*
Jingru Sun, *Department of Geosciences, Princeton University, Princeton, NJ, USA*
Gabriel Vecchi, *Department of Geosciences, Princeton University, Princeton, NJ, USA; High Meadows Environmental Institute, Princeton University, Princeton, NJ, USA*
Friederike E. L. Otto, *Grantham Institute, Imperial College London, UK*

Main findings

- The flooding and landslides leading to severe impacts were a direct consequence of extremely heavy rainfall in the week beginning on 23rd May and continuing into June. We therefore assess the role of climate change in 7 & 15-day mean rainfall.
- While the full profile of the impacts on human life and livelihoods has yet to be analysed, initial assessments show that the floods and particularly landslides disproportionately affected vulnerable communities, with particular devastation in low-income neighbourhoods. Thus, the magnitude of this disaster on these groups has been exacerbated by pre-existing structural vulnerability in the region.
- Today, there is a dense network of 389 weather stations in the area. However, we select 75 stations that have consistent data since at least the 1970s and are distributed across the study region for our observational analysis. Both the 7- and 15-day events are exceptionally rare events, which have only approximately a 1-in-500 and 1-in-1000 chance respectively of happening in any year in today's climate, which has been warmed about 1.2°C by human activities.
- Although they are still very unusual, these events are now more likely to happen than they would have been in a climate that had not been warmed by human activities. But, as both events are far outside the previously observed records, it is not possible to quantify how much more likely climate change has made them to happen, based on observations. Warming of the planet has also increased the intensity of the rainfall: rainfall events as rare as these, that occurred in a 1.2°C cooler climate, would have been approximately a fifth less intense.
- To determine the role of climate change in these observed changes we undertake the same assessment using climate models. While many climate models are able to simulate the main precipitation features over the region, we find that for this spatially small event, all models exhibit systematic errors in precipitation magnitudes, partly due to having coarse spatial resolution and misrepresentation of key physical processes (e.g. convection). We can therefore not quantify the role of climate change in the observed increase in likelihood and intensity.
- However, combining observations with our physical understanding of the climate system we conclude that human-caused climate change is, at least in part, responsible for the observed increases in likelihood and intensity of heavy rainfall events as observed in May 2022.
- These findings are consistent with future projections of heavy rainfall in the region and suggest that these trends will continue to increase as long as greenhouse gas concentrations continue to increase. Also, due to climate change, other factors such as rising sea levels and higher tides could increase the vulnerability to heavy rainfall, leading to more urban floods in Recife, for example.
- The extreme nature of the floods made it so that exposure was the main determinant of impact, although long-term impacts and recovery will likely be mediated by socio-economic, demographic and governance factors. An increase in urbanisation, especially unplanned and informal in low-lying flood-prone areas and steep hillsides

have increased the community exposure to these hazards. While forecasts and warnings were provided, it is unclear to what extent these informed anticipatory or early action that could have reduced the impacts.

- This indicates the need to review and strengthen the linkage between weather warnings and the process that would lead to anticipatory action based on those warnings. This region also generally has an infrastructure deficit (e.g. housing, roads, water and sanitation etc.). As new infrastructure is built, there is an opportunity to increase resilience by accounting for increasing risks in the design and location, instead of reverting to outdated design standards.

1 Introduction.

The combination of high spatial and temporal rainfall variability and the highest proportion of people living in poverty in Brazil makes the Northeast of Brazil (NEB) particularly vulnerable to climate variability, extremes and climate change impacts. Furthermore, there is strong evidence that climate change will increase drought risk and severity in this region (IPCC, 2021¹). Although the NEB has historically been known for extreme droughts, heavy rainfall events also have a history of severely impacting the area. In the week beginning on May 23rd, 2022, very heavy rainfall started falling over parts of NEB, in the states of Pernambuco, Alagoas, and Paraíba. The states of Sergipe and Rio Grande do Norte were also affected by this event. The rainfall began to intensify on the 25th of May, leading to flash floods and landslides in NEB and a dam break in the state of Paraíba (FloodList, 26 May 2022²). In less than 24 hours on May 27-28, parts of Pernambuco received about 70% of the total rainfall expected for the entire month of May (France24, 30 May 2022³). Fig. 1 shows this event, averaged over the week when most of the associated impacts were reported (Fig. 1(a)) and over the fortnight when the precipitation was high.

1

https://www.ipcc.ch/report/ar6/wg1/downloads/factsheets/IPCC_AR6_WGI_Regional_Fact_Sheet_Central_and_South_America.pdf

² <https://floodlist.com/america/brazil-floods-pernambuco-alagoas-paraiba-may-2022#>

³

<https://www.france24.com/en/live-news/20220530-bolsonaro-visits-disaster-zone-after-deadly-brazil-rains>

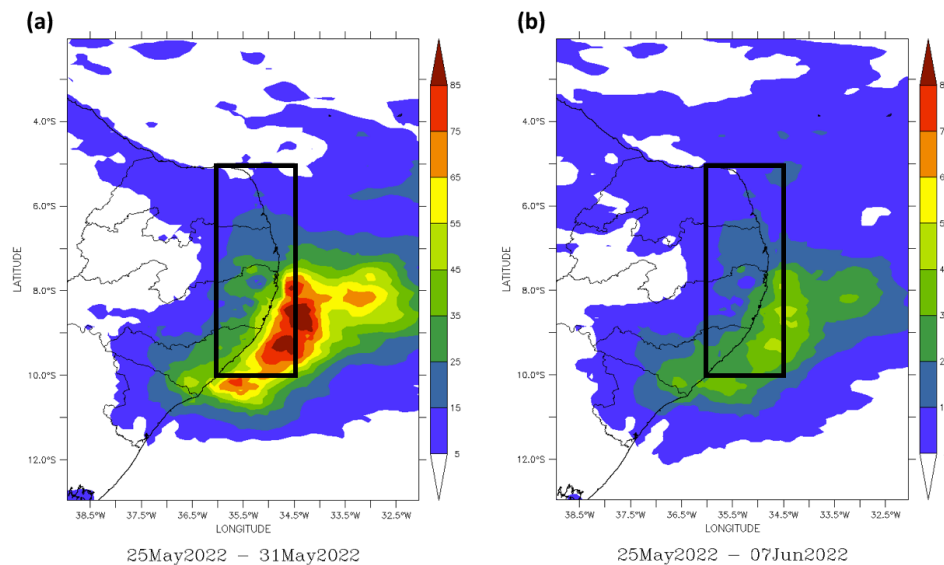


Figure 1: (a) Observed average 7-day rainfall for 25-31 May 2022 and (b) 15-day rainfall for 25 May-1 June, 2022, over North Eastern Brazil from MERGE-GPM dataset.

This event triggered extensive landslides and widespread floods in the affected areas, resulting in 133 fatalities and over 25,000 displaced, predominantly impacting residents of low-income neighbourhoods near hillsides (Gizmodo, 1 June 2022⁴). Following the disaster, at least 80 municipalities across Pernambuco and Alagoas declared a state of emergency (Civil Defense Pernambuco, 2022; Civil Defense Alagoas, 2022). The Metropolitan Region of Recife (RMR) in the state of Pernambuco was badly hit, this event being one of the worst extreme rainfall events in its history.

Easterly waves, that are typical to this season and have the potential to cause heavy and widespread rainfall as well as thunderstorms, was the primary driver of this event. The incidence of this phenomenon when this part of the country had already been experiencing wetter than normal rainfall conditions, associated with a warm tropical South Atlantic and La Niña conditions over the Pacific, led to the abnormally high rainfall amounts in this region. The impacts due to heavy rainfall in these parts, especially flooding, are known to be exacerbated when the rainfall concurs with high astronomical tides, storm surges and run ups, and also influenced by sea level rise associated with climate change (Costa et al., 2010). However, the impacts of the May 2022 event is largely ascribed to the precipitation itself (France24, 28 May 2022⁵).

⁴ <https://gizmodo.com/brazil-landslides-recife-pernambuco-floods-1848997858>

⁵ <https://www.france24.com/en/live-news/20220528-downpours-in-brazil-leave-at-least-28-dead>

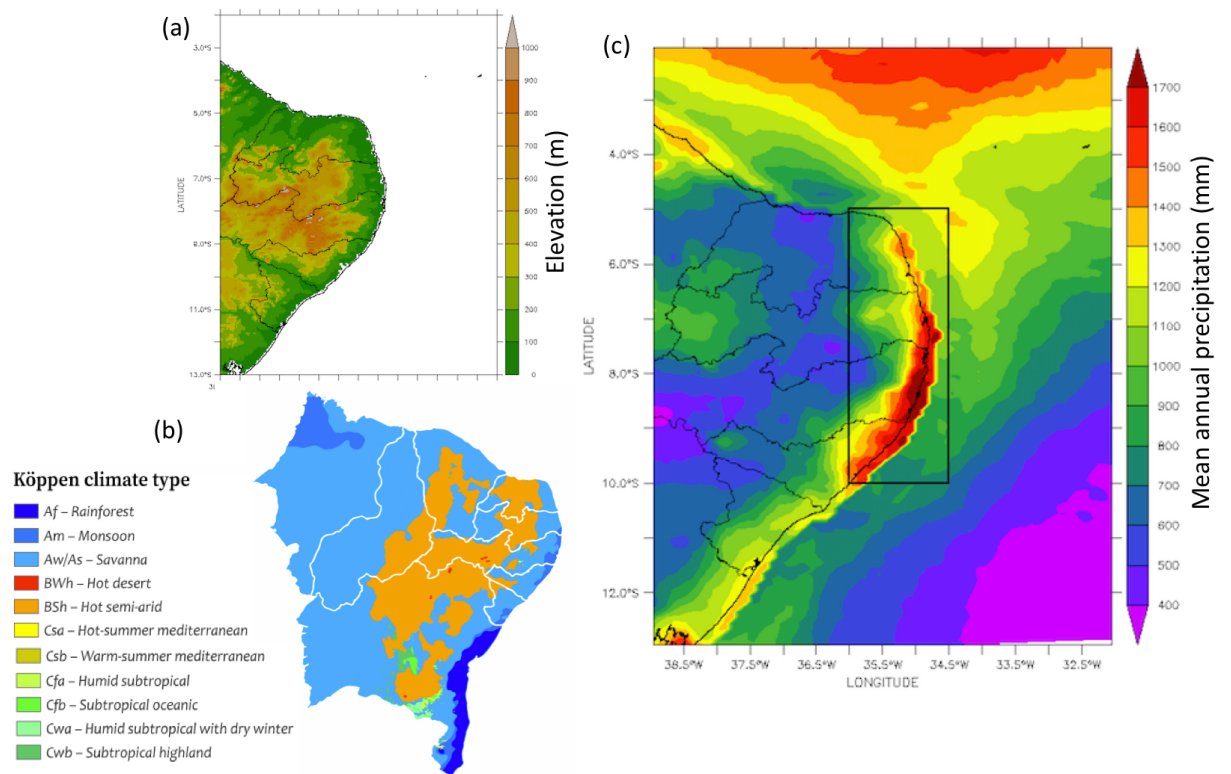


Figure 2. (a) Topography of the region, with ocean displayed as white area and state borders indicated by black lines. (b) Köppen Climate Zones in Northeast Brazil (Alvarez et al. 2012). (c) Annual mean precipitation (mm) over Northeast Brazil from MERGE-GPM dataset (Rozante et al. 2010). The study region is indicated by the black box.

In this study, we analyse precipitation over a small region enclosing the area with the highest impacts. Recognising the localised nature of the rainfall, for this analysis, we restrict to using models only of high resolution ($\leq 60\text{km}$). However, the resolution of these models is still such that very few grid boxes represent the coastal region with the largest impacts. In order to be able to use these models and compare with observations, we choose to extend the region slightly further inland. The chosen spatial definition is a rectangular domain defined by 10°S - 5°S ; 36°W - 45.5°W , in which we use land points only in the black box in Fig. 1. Consideration is also given to the homogeneity of the region (Fig. 2(a)). The study box is dominated by one type of climate zone - the tropical Savanna (Fig. 2(b)) and lies to the east of a drier region in climatological precipitation (Fig. 2(c)). Because the maximum impacts were witnessed in one week, we use as a temporal definition the annual maximum 7-day average precipitation from, RX7d. Because the event is furthermore characterised by higher than average precipitation over periods longer than a week, with several peaks, we also use the alternative temporal definition of the annual maximum of 15-day average precipitation, RX15d.

The period from March to August is the rainy season of the eastern northeast Brazil coast. Generally, in March and April the Intertropical Convergence Zone (ITCZ) has its largest incursion to the south hemisphere and in its seasonal march produces rainfall events over the whole Northeast Brazil region through deep convection and the so-called cold rain (Waliser; Jiang, 2015). On the other hand, the rainfall over the eastern coast of Northeast Brazil is

largely produced by easterly wave disturbances (Gomes et al., 2015). Even though these waves occur all year round, they have a peak of activity during the months of May to August, reaching the coast with heavy rain and with rainfall events lasting for a few days. They have a spatial scale of local-regional action and very often are associated with warm convective rainfall (Liu and Zipser, 2009). These characteristics are hard to be represented in climate models due to the lack of high spatial resolution and adequate convection schemes. Expressive daily rainfall amounts over 150 mm are commonly recorded in this region and are usually associated with easterly wave disturbances (Gomes et al., 2015). For example, from 21-May until 01-Jun 2017, some cities in Pernambuco experienced consecutive days with very high daily rainfall records. Other recent events that were also associated with severe impacts in Pernambuco include those recorded in the years 2000, 2004, 2005, 2010, 2011, 2017, 2019 and 2021⁶.

So far, not many attribution studies for floods or extreme precipitation events have been carried out for regions in Northeast Brazil. One recent study by Rudorff et al. (2021) has assessed river floods from the Parnaíba river, situated in a different climate zone to the west of our study region, that occurred in the year 2018, 2019 and 2022, the authors found that anthropogenic factors have increased the likelihood of these events by approximately 30%, although the link to observed (decreasing) trends is not clear.

2 Data and methods

2.1 Observational data

Station data

We analysed long-term observed daily precipitation records from 1960-present, from 389 weather stations spread over our study region, as shown in Fig. 3(a). The data is sparse in the beginning of the time series, and becoming denser from the 80's. These stations are owned and monitored by the meteorology/hydrology state service institutions in the states of Rio Grande do Norte, Paraíba, Pernambuco and Alagoas- Empresa de Pesquisa Agropecuária do Rio Grande do Norte⁷ (EMPARN-RN), Agência Executiva de Gestão das Águas⁸ (AESA), Agência Pernambucana de Águas e Clima⁹ (APAC-PE) and Secretaria do Estado do Meio Ambiente e Recursos Hídricos de Alagoas¹⁰ (SEMARH-AL) and federal institutions- Instituto Nacional de Meteorologia¹¹ (INMET) and Agência Nacional de Águas e Saneamento Básico¹² (ANA).

The time series of these 389 stations have been averaged to represent the average precipitation over the area. However, to avoid spurious trends due to inhomogeneity in the number of stations available in time, we also averaged over the 75 stations that have data from at least

⁶ <https://www.pe-az.com.br/o-estado/fenomenos-naturais/1400-enchentes>

⁷ www.emparn.rn.gov.br

⁸ <http://www.aesa.pb.gov.br>

⁹ <https://www.apac.pe.gov.br>

¹⁰ <http://www.semarh.al.gov.br>

¹¹ <https://portal.inmet.gov.br>

¹² <https://www.gov.br/ana/en>

from 1970 until May 2022, and over the 11 stations with data from 1960 until now (a subset of the 75 stations). The distribution of the 75 station locations is relatively equally spaced (Fig. 3(b)), whereas the 11 stations with the longest data are concentrated over a small region (Fig. 3(c)).

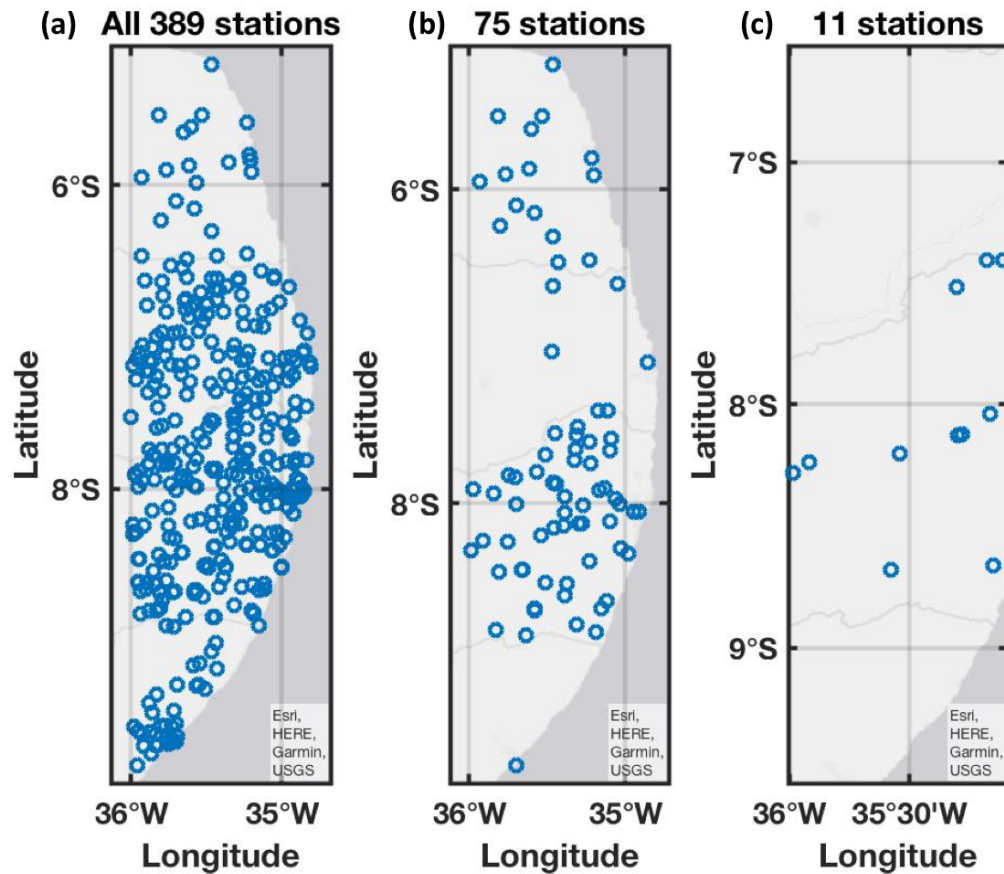


Figure 3. Locations of weather stations within the study region. (a) All 389 stations (b) 75 stations with data from at least 1970. (c) 11 stations with data since 1960 (subset of 75 stations in panel (b)).

We compare the annual 7-day maxima and annual 15-day maxima of the three different station averages with ERA5 data (Hersbach et al. 2020) and GPM-Merge (Rozante et al. 2010) averaged over the study area (see Fig. 4). The GPM-Merge dataset is only used for this comparison, as it is too short for an extreme value analysis. The ERA5 data differs from the other time series and is therefore considered to be less reliable for this specific region. The 75 stations average resembles the average over 389 stations well over most of the years and results between the 389 stations average and the 75 stations average are consistent (not shown). The 11 stations average diverges from the other time series. This may have to do with the unequal distribution of these stations across the region, being located in a small subregion of the full rectangular study area. Therefore the 11 stations average is not considered for further analysis. We thus continue the analysis of observations with the 75 stations average.

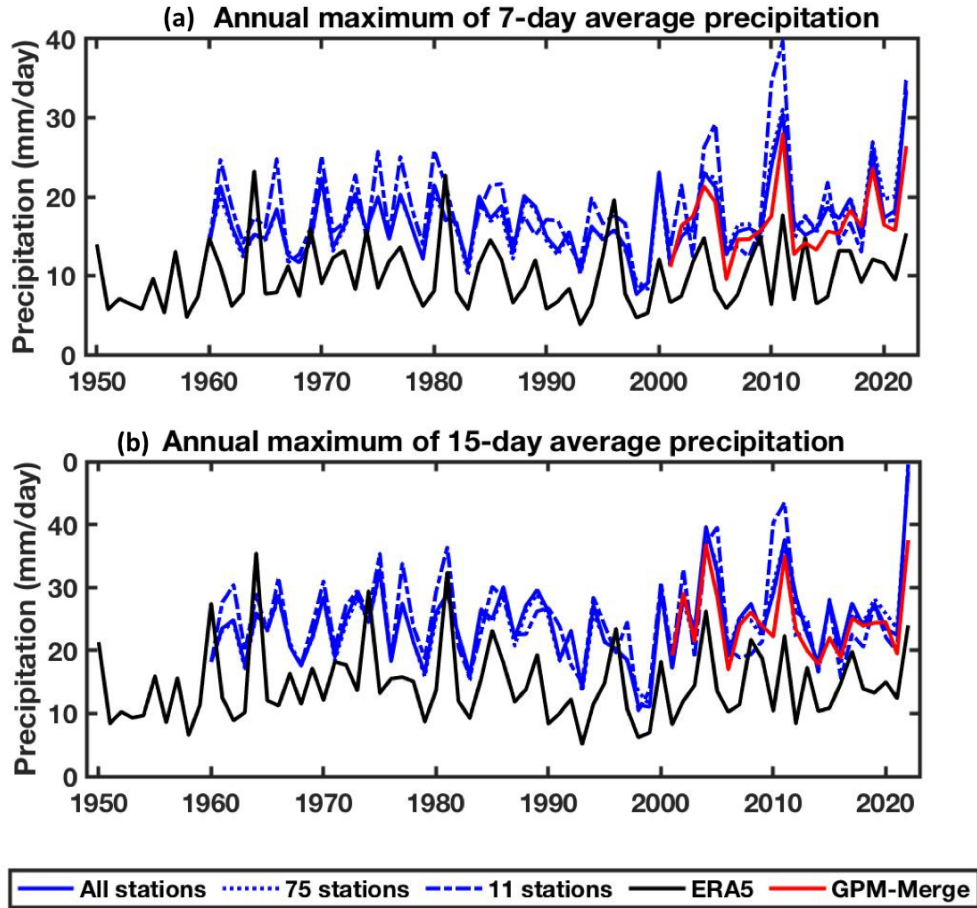


Figure 4: (a) Time series of annual 7-day maximum precipitation in [mm/day] and (b) 15-day maximum precipitation in [mm/day] for different selections of stations (all, 75 or 11) and two different observations/reanalyses (ERA5, GPM-Merge).

As a measure of anthropogenic climate change we use the (low-pass filtered) global mean surface temperature (GMST), where GMST is taken from the National Aeronautics and Space Administration (NASA) Goddard Institute for Space Science (GISS) surface temperature analysis (GISTEMP, Hansen et al., 2010 and Lenssen et al. 2019).

2.2 Model and experiment descriptions

We use three different multi-model ensembles from climate modelling experiments using very different framings (Philip et al., 2020): Sea Surface temperature (SST) driven global circulation high resolution models and coupled global circulation models and regional climate models.

The first set of models used in the analysis include the AM2.5C360 (Yang et al. 2021, Chan et al. 2021) and the FLOR (Vecchi et al. 2014) climate models developed at Geophysical Fluid Dynamics Laboratory (GFDL). The AM2.5C360 is an atmospheric GCM based on that in the FLOR model (Delworth et al. 2012, Vecchi et al. 2014) with a horizontal resolution of 25 km. Ten ensemble simulations of the Atmospheric Model Intercomparison Project (AMIP)

experiment (1871-2020) are analysed. These simulations are initialised from ten different pre-industrial conditions but forced by the same SSTs from HadISST1 (Rayner et al. 2003) after groupwise adjustments (Chan et al. 2021), as well as the same historical radiative forcings. The FLOR model, on the other hand, is an atmosphere-ocean coupled GCM with a resolution of 50 km for land and atmosphere and 1 degree for ocean and ice. Five ensemble simulations from FLOR are analysed, which cover the period from 1860 to 2100 and include both the historical and RCP4.5 experiments driven by transient radiative forcings from CMIP5 (Taylor et al. 2012).

The second ensemble is the HighResMIP SST-forced model ensemble (Haarsma et al. 2016), the simulations for which span from 1950 to 2050. The SST and sea ice forcings for the period 1950-2014 are obtained from the 0.25° x 0.25° Hadley Centre Global Sea Ice and Sea Surface Temperature dataset that are area-weighted re-gridded to match the climate model resolution (see Table 1). For the ‘future’ time period (2015-2050), SST/sea-ice data are derived from RCP8.5 (CMIP5) data, and combined with greenhouse gas forcings from SSP5-8.5 (CMIP6) simulations (see Section 3.3 of Haarsma et al. 2016 for further details).

Table 1: List of HighResMIP models used in the study.

| Model | Resolution | Institute |
|-----------------|------------|---|
| CNRM-CM6-1-HR | ~50 km | Centre National de Recherches Météorologiques |
| EC-Earth3P-HR | ~40 km | EC-Earth-Consortium |
| HadGEM3-GC31-HM | ~25 km | UK Met Office, Hadley Centre |
| HadGEM3-GC31-MM | ~60 km | UK Met Office, Hadley Centre |

The third ensemble is the Coordinated Regional Climate Downscaling Experiment CORDEX-CORE (10 models with at 0.44° resolution (SAM-44) and 4 models at 0.22° resolution (SAM-22)) multi-model ensemble (Gutowski et al., 2016; Giorgi et al., 2021), comprising 14 simulations resulting from pairings of Global Climate Models (GCMs) and Regional Climate Models (RCMs) (see Table 2 below). These simulations are composed of historical simulations up to 2005, and extended to the year 2100 using the RCP8.5 scenario.

Table 2. List of regional climate models used with their driving global climate models (see Gutowski et al., 2016 for a description of the Cordex experiment and Taylor et al. (2012) for a description of the GCMs)

| Regional Climate Model | Resolution | Global Climate Model | Period |
|------------------------|------------|----------------------|-----------|
| REMO2015 | 0.22° | MPI-ESM-LR | 1970-2100 |
| REMO2015 | 0.22° | NorESM1-M | 1970-2100 |
| RegCM4-7 | 0.22° | MPI-ESM-MR | 1970-2099 |
| RegCM4-7 | 0.22° | NorESM1-M | 1970-2099 |

| | | | |
|--------------|-------|---------------|-----------|
| REMO2009 | 0.44° | MPI-ESM-LR | 1950-2100 |
| SMHI-RCA4 | 0.44° | CSIRO-Mk3-6-0 | 1951-2100 |
| SMHI-RCA4 | 0.44° | EC-EARTH | 1951-2100 |
| SMHI-RCA4 | 0.44° | IPSL-CM5A-MR | 1951-2099 |
| SMHI-RCA4-7 | 0.44° | MIROC5 | 1951-2099 |
| SMHI-RCA4 | 0.44° | HadGEM2-ES | 1951-2100 |
| SMHI-RCA4 | 0.44° | MPI-ESM-LR | 1951-2100 |
| SMHI-RCA4 | 0.44° | NorESM1-M | 1951-2100 |
| SMHI-RCA4 | 0.44° | GFDL-ESM2M | 1951-2100 |
| UCAN_WRF341I | 0.44° | CanESM2 | 1950-2100 |

The 1960-2022 period for which the observed data is available is chosen for model evaluation, while the entire length of simulations upto the year 2022 is considered for the attribution analysis.

2.3 Statistical methods

In this analysis we analyse precipitation time series from eastern Northeast Brazil coast for 7-day and 15-day annual maxima where long records of observed data are available. Methods for observational and model analysis and for model evaluation and synthesis are used according to the World Weather Attribution Protocol, described in Philip et al. (2020), with supporting details found in van Oldenborgh et al. (2021), Ciavarella et al. (2021) and [here](#).

The analysis steps include: (i) trend calculation from observations; (ii) model validation; (iii) multi-method multi-model attribution and (iv) synthesis of the attribution statement.

We calculate the return periods, Probability Ratio and change in intensity of the event under study for the comparison between observed GMST values of 2022 and past GMST values (1850-1900, based on the Global Warming Index <https://www.globalwarmingindex.org>), which is a difference of 1.2 °C. To statistically model the event under study, we use a generalised extreme value (GEV) that scales with GMST. Next, results from observations and models that pass the validation tests are synthesised into a single attribution statement.

3 Observational analysis: return time and trend

3.1 Analysis of point station data

Fig. 5(a-b) shows the time series of the station-averaged annual maximum precipitation including the 10-year running mean. The magnitudes of the May 2022 event- 33.96 mm/day

for the 7-day event and 23.95 mm/day for the 15-day event, are the highest in the respective records, as can be seen in these figures.

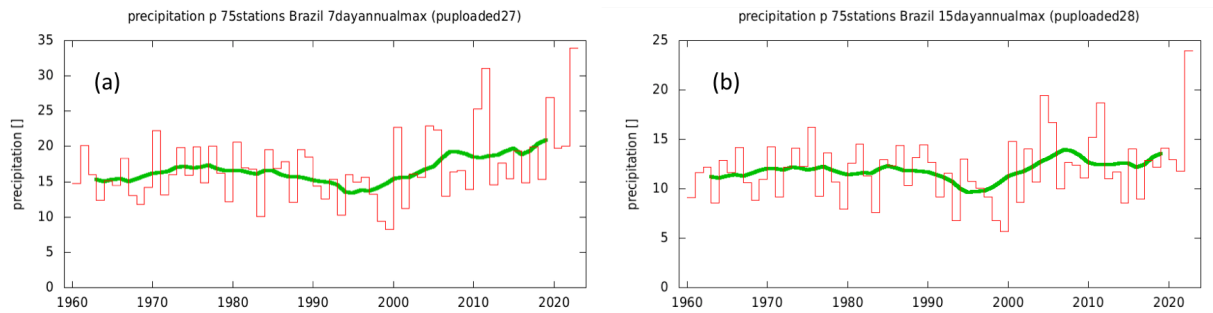


Figure 5: Time series of annual (a) 7-day maximum precipitation in [mm/day] and (b) 15-day maximum precipitation in [mm/day] averaged over the selected 75 precipitation stations and the corresponding GEV fits. The green line shows the 10-year running mean.

Fig. 6(a) shows the response of annual maximum 7-day average precipitation to the global mean surface temperature, while Fig. 6(b) shows the return period curve of the 7-day event in the current climate and in the past climate when the global mean temperature was 1.2 °C cooler. The return period of such an event in the current climate is 500 years (95% Confidence Interval (CI) 66 years to ∞). The positive trend in panel (a) indicates a tendency towards more and heavier precipitation events in recent years. The probability ratio is 43000 (95% CI 1.7 to ∞) and equivalently, the intensity change is 27% (95% CI 0.95% to 59%). Fig. 6(c-d) shows the trends and the GEV-fits based on the 15-day event definition. The return period in this case is found to tend to ∞ (lower bound of 240,000 years), which implies that a 15-day event of this magnitude is very extreme even for the current climate which is 1.2 °C warmer than pre-industrial. Consequently, the probability ratio also cannot be defined. The intensity change ranges from 16-38.5% (at 95%CI) with a best estimate of 13%.

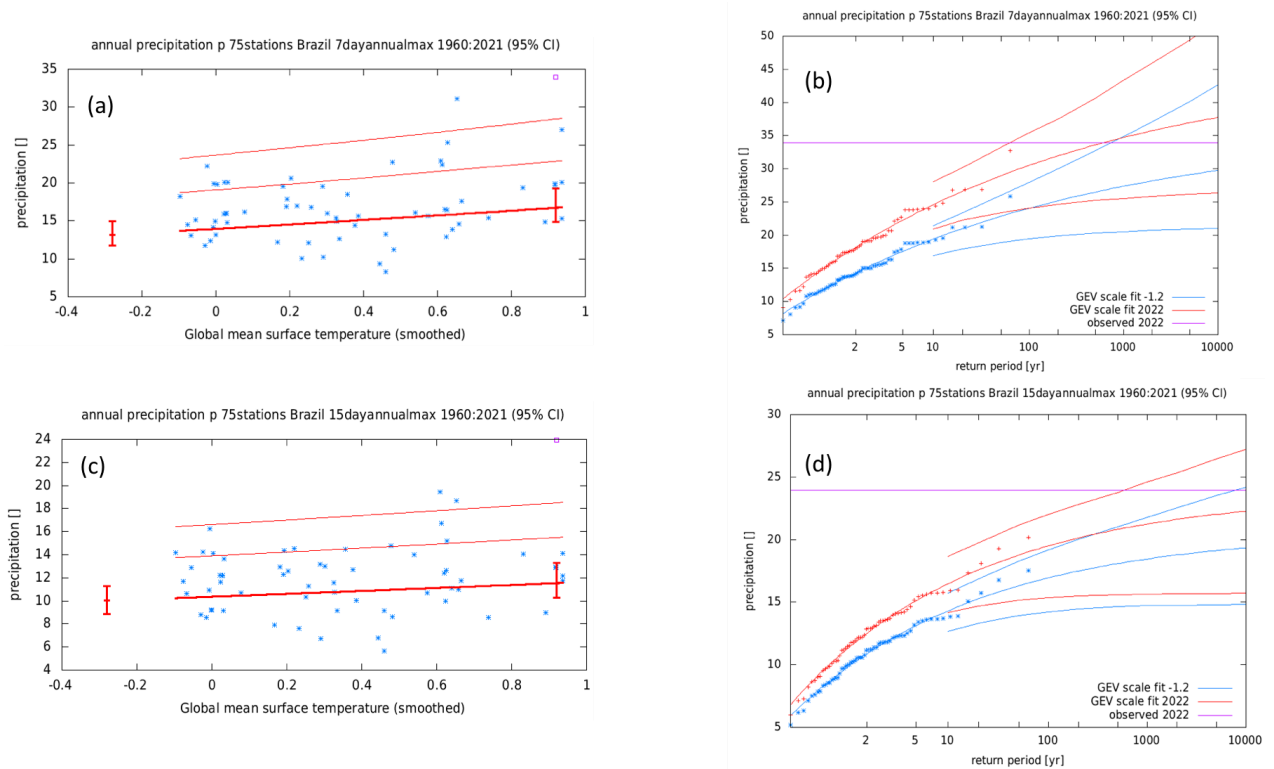


Figure 6: (a) GEV fit with constant dispersion parameter, and location parameter scaling proportional to GMST, for the average over 75 stations. No information from 2022 is included in the fit. **Left:** Annual 7-day (a) and 15-day (c) average rainfall as a function of the smoothed GMST. The thick red line denotes the time-varying location parameter. The vertical red lines show the 95% confidence interval for the location parameter, for the current, 2022 climate and the fictional, 1.2°C cooler climate. The 2022 observation is highlighted with the magenta box. **Right:** Return time plots for the climate of 2022 (red) and a climate with GMST 1.2 °C cooler (blue), for the 7-day average (b) and the 15-day average (d). The past observations are shown twice: once shifted up to the current climate and once shifted down to the climate of the late nineteenth century. The markers show the data and the lines show the fits and uncertainty from the bootstrap. The magenta line shows the magnitude of the 2022 event analysed here.

For ascertaining that there are no inconsistencies in the results arising from (i) the choice of the subset of 75 representative stations (Fig. 3b) instead of all 389 stations (Fig. 3a) for reasons explained in Section. 2.1, and (ii) the choice of time series to include the 1960-1969 period when the stations were sparse and concentrated to a smaller region (Fig. 3c), we repeat the above analysis for the 7-day and 15-day events, for two additional cases-

1. Considering all 389 stations for 1960-2022 (plots shown in Fig. S5).
2. Considering 75 stations for 1970-2022 (plots shown in Fig. S6).

We find that there is no indication of differences in the estimates for return period of the 2022 event, probability ratio and change in intensity between any of these cases.

3.2 Influence of modes of natural variability

During the period of heavy precipitation and the preceding months there has been an ongoing La Niña event (Jones, 2022). This modulates the rainfall and it may have exacerbated the average rainfall in the eastern Northeast Brazil (ENEB). Fig. 7 shows the correlations between the combined GPCP v2020 + monitoring product V6 + first guess (Schneider et al., 2020; Ziese et al., 2011) and the NCEPv5 ERSST Sea Surface Temperature (SST) values (Huang et al., 2017). SST values in the Southern Atlantic ocean were only slightly higher in May, so this may have had an influence as well. In the ENEB, the precipitation is also modulated by Easterly Waves Disturbances (EWD) (Gomes et al., 2015; Kouadio et al., 2012; Ramos, 1975; Torres & Ferreira, 2011) with maximum rainfall between May and July, and annual average precipitation above 1500 mm. SST anomalies over Tropical South Atlantic (TSA) and El Niño Southern Oscillation (ENSO) that interact with global circulation modulate the rainfall variability in the ENEB (Andreoli & Kayano, 2007; Silva et al., 2018; Silva & Guedes, 2012, Torres & Ferreira, 2011; Rodrigues et al. 2020). The very intense daily rainfall events of May 2022 were largely caused by the propagation EWD (Gomes et al., 2015), which in combination with an anomalously warm tropical Atlantic and a humid and unstable atmosphere near the east coast of Northeast Brazil favoured the development of convective precipitation clouds in a sequence of days.

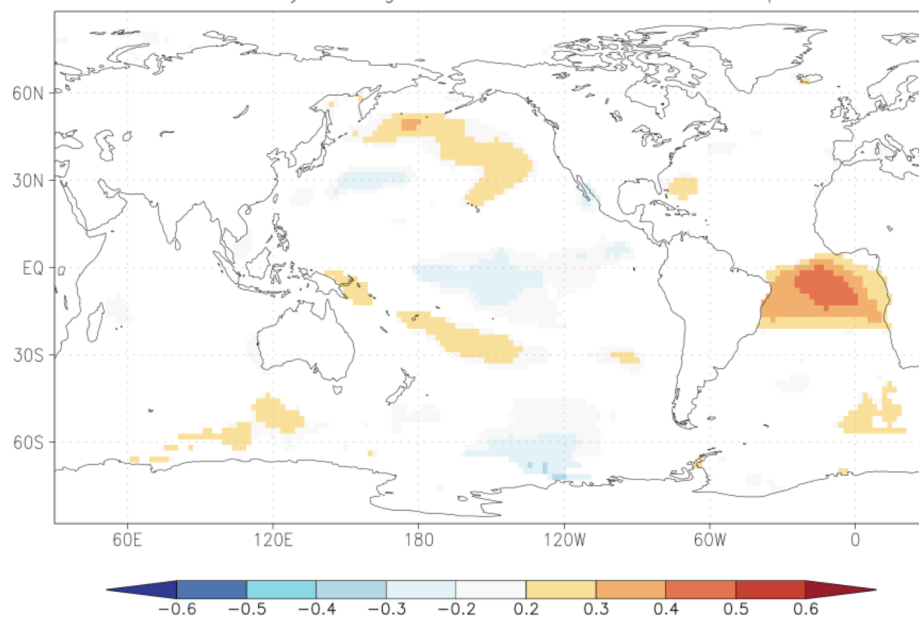


Figure 7: Correlation between rainfall (from GPCP dataset) over the region in Brazil and global ERSST Sea Surface Temperatures for months Mar-May 2022, calculated over years 1891-2022.

4 Model evaluation

In the subsections below we show the results of the model validation for the 7-day and the 15-day events. The seasonal cycle is labelled 'reasonable' if it has one peak extending in time

to at least May. We note that the warm rains are not represented well in most of the models, with the precipitation seasonal cycles declining around May, thus missing the warm rain season from May-Aug. The only exception is CNRM-CM6-1-HR from the HighResMIP experiment, where the seasonal cycle is consistent with the observed cycle (Fig. S1 for observations; Fig. S3 (a-c) for climate models).

Table3. Evaluation results for the climate models considered for the attribution analysis of annual maximum 7-day rainfall in the year 2022, over the study region. The table contains qualitative assessments of seasonal cycle and spatial pattern of precipitation from the models (good, reasonable, bad) along with estimates for dispersion parameter, shape parameter and event magnitude. The corresponding estimates for observations are shown in blue. Based on overall suitability, the models are classified as good, reasonable and bad, shown by green, yellow and red highlights, respectively.

| Observations | Seasonal cycle | Spatial pattern | Dispersion | Shape parameter | Event magnitude |
|---|----------------|-----------------|-----------------------------|-----------------------------|---------------------------------------|
| Station | | | 0.243 (0.187 ... 0.293) | -0.14 (-0.43 ... 0.019) | 33.95 |
| Model | | | | | Threshold for 500-yr return period |
| FLOR historical-rcp45 (5) | reasonable | good | 0.272 (0.248 ... 0.292) | -0.049 (-0.12 ... 0.017) | 45.188 |
| CNRM-CM6-1-HR HighResMIP (1) | good | good | 0.190 (0.157 ... 0.215) | -0.042 (-0.21 ... 0.10) | 27.773 |
| EC-Earth3P-HR HighResMIP (1) | reasonable | good | 0.298 (0.230 ... 0.347) | 0.046 (-0.15 ... 0.21) | 19.848 |
| HadGEM3-GC31-HM HighResMIP (1) | reasonable | reasonable | 0.265 (0.199 ... 0.311) | -0.12 (-0.29 ... 0.066) | 38.075 |
| HadGEM3-GC31-MM HighResMIP (1) | reasonable | reasonable | 0.306 (0.245 ... 0.355) | 0.088 (-0.10 ... 0.21) | 45.157 |
| AM2.5C360 AMIP (10) | reasonable | good | 0.291 (0.274 ... 0.313) | -0.042 (-0.12 ... 0.011) | 47.952 |
| MPI-ESM-LR / REMO2015 CORDEX SAM-22 (1) | bad | bad | 0.161 (0.115 ... 0.191) | -0.13 (-0.46 ... 0.089) | 33.551 |
| NorESM1-M / REMO2015 CORDEX SAM-22 (1) | reasonable | reasonable | 0.230 (0.179 ... 0.269) | 0.027 (-0.34 ... 0.23) | 29.41 |
| MPI-ESM-MR / RegCM4-7 CORDEX SAM-22 (1) | bad | bad | 0.428 (0.333 ... 0.489) | 0.35 (0.079 ... 0.73) | 233.28 |
| NorESM1-M / RegCM4-7 CORDEX SAM-22 (1) | reasonable | reasonable | 0.568 (0.442 ... 0.662) | -0.29 (-0.70 ... 0.059) | 79.042 |
| MPI-ESM-LR / REMO2009 CORDEX SAM-44 (1) | bad | bad | 0.145 (0.114 ... 0.171) | 0.028 (-0.15 ... 0.19) | 41.279 |
| CSIRO-Mk3-6-0 / SMHI-RCA4 CORDEX SAM-44 (1) | bad | bad | 0.120 (0.0950 ... 0.139) | -0.0020 (-0.23 ... 0.23) | 11.452 |
| EC-EARTH / SMHI-RCA4 CORDEX SAM-44 (1) | bad | bad | 0.176 (0.128 ... 0.205) | 0.24 (0.026 ... 0.49) | 67.528 |
| IPSL-CM5A-MR / SMHI-RCA5 CORDEX SAM-44 (1) | reasonable | bad | 0.262 (0.204 ... 0.308) | -0.14 (-0.34 ... 0.016) | 50.407 |
| MIROC5 / SMHI-RCA4 CORDEX SAM-44 (1) | reasonable | reasonable | 0.335 (0.268 ... 0.387) | 0.045 (-0.17 ... 0.24) | 58.86 |

| | | | | | |
|--|------------|------------|-------------------------|-------------------------|--------|
| HadGEM2-ES / SMHI-RCA4 CORDEX SAM-44 (1) | reasonable | reasonable | 0.313 (0.236 ... 0.378) | -0.36 (-0.54 ... -0.24) | 37.861 |
| MPI-ESM-LR / SMHI-RCA4 CORDEX SAM-44 (1) | bad | bad | 0.202 (0.154 ... 0.236) | -0.078 (-0.29 ... 0.11) | 40.587 |
| NorESM1-M / SMHI-RCA4 CORDEX SAM-44 (1) | reasonable | reasonable | 0.383 (0.301 ... 0.442) | -0.13 (-0.34 ... 0.021) | 43.636 |
| GFDL-ESM2M / SMHI-RCA4 CORDEX SAM-44 (1) | bad | bad | 0.294 (0.223 ... 0.351) | 0.24 (-0.10 ... 0.58) | 117.06 |
| CanESM2/ UCAN_WRF341I CORDEX SAM-44 (1) | reasonable | reasonable | 0.393 (0.300 ... 0.460) | 0.14 (-0.017 ... 0.31) | 54.355 |

Table 4. Evaluation results for the climate models considered for the attribution analysis of annual maximum 15-day rainfall in the year 2022, over the study region. The table contains qualitative assessments of seasonal cycle and spatial pattern of precipitation from the models (good, reasonable, bad) along with estimates for dispersion parameter, shape parameter and event magnitude. The corresponding estimates for observations are shown in blue. Based on overall suitability, the models are classified as reasonable and bad, shown by yellow and red highlights, respectively.

| Observations | Seasonal cycle | Spatial pattern | Dispersion | Shape parameter | Event magnitude |
|---|---------------------------------------|-----------------|--------------------------|---------------------------|-------------------------------------|
| Station | | | 0.243 (0.188 ... 0.290) | -0.23 (-0.48 ... -0.084) | 23.95 |
| Model | | | | | Threshold for 1000-yr return period |
| FLOR historical-rcp45 (5) | reasonable, drops early in the season | good | 0.235 (0.213 ... 0.249) | -0.078 (-0.20 ... -0.029) | 31.702 |
| CNRM-CM6-1-HR HighResMIP (1) | good | good | 0.142 (0.111 ... 0.168) | 0.089 (-0.10 ... 0.24) | 25.141 |
| EC-Earth3P-HR HighResMIP (1) | reasonable | good | 0.271 (0.210 ... 0.315) | -0.011 (-0.23 ... 0.17) | 14.484 |
| HadGEM3-GC31-HM HighResMIP (1) | reasonable | reasonable | 0.257 (0.182 ... 0.305) | -0.14 (-0.32 ... 0.048) | 28.53 |
| HadGEM3-GC31-MM HighResMIP (1) | reasonable | reasonable | 0.275 (0.227 ... 0.313) | 0.073 (-0.11 ... 0.21) | 32.734 |
| AM2.5C360 AMIP (10) | reasonable, drops early in the season | good | 0.277 (0.254 ... 0.299) | -0.043 (-0.11 ... 0.017) | 37.222 |
| MPI-ESM-MR/ REMO2015 CORDEX SAM-22 (1) | bad | bad | 0.159 (0.113 ... 0.194) | -0.18 (-0.48 ... 0.047) | 27.019 |
| NorESM1-M / REMO2015 CORDEX SAM-22 (1) | reasonable | reasonable | 0.246 (0.188 ... 0.288) | -0.15 (-0.38 ... 0.018) | 18.967 |
| MPI-ESM-MR / RegCM4-7 CORDEX SAM-22 (1) | bad | bad | 0.341 (0.259 ... 0.401) | 0.32 (0.077 ... 0.58) | 147.17 |
| NorESM1-M / RegCM4-7 CORDEX SAM-22 (1) | reasonable | reasonable | 0.578 (0.459 ... 0.674) | -0.21 (-0.79 ... 0.21) | 60.047 |
| MPI-ESM-LR / REMO2009 CORDEX SAM-44 (1) | bad | bad | 0.196 (0.153 ... 0.231) | -0.19 (-0.39 ... 0.015) | 28.936 |
| CSIRO-Mk3-6-0 / SMHI-RCA4 CORDEX SAM-44 (1) | bad | bad | 0.117 (0.0920 ... 0.139) | 0.030 (-0.22 ... 0.27) | 10.389 |

| | | | | | |
|--|------------|------------|-------------------------|--------------------------|--------|
| EC-EARTH / SMHI-RCA4 CORDEX SAM-44 (1) | bad | bad | 0.163 (0.127 ... 0.190) | 0.10 (-0.18 ... 0.33) | 42.4 |
| IPSL-CM5A-MR / SMHI-RCA5 CORDEX SAM-44 (1) | reasonable | bad | 0.251 (0.180 ... 0.301) | -0.12 (-0.30 ... 0.062) | 41.431 |
| MIROC5 / SMHI-RCA4 CORDEX SAM-44 (1) | reasonable | reasonable | 0.257 (0.211 ... 0.306) | -0.095 (-0.46 ... 0.14) | 32.603 |
| HadGEM2-ES / SMHI-RCA4 CORDEX SAM-44 (1) | reasonable | reasonable | 0.311 (0.238 ... 0.379) | -0.39 (-0.75 ... -0.26) | 27.893 |
| MPI-ESM-LR / SMHI-RCA4 CORDEX SAM-44 (1) | bad | bad | 0.221 (0.175 ... 0.263) | -0.18 (-0.51 ... -0.012) | 30.67 |
| NorESM1-M / SMHI-RCA4 CORDEX SAM-44 (1) | reasonable | reasonable | 0.355 (0.273 ... 0.416) | -0.068 (-0.28 ... 0.12) | 34.438 |
| GFDL-ESM2M / SMHI-RCA4 CORDEX SAM-44 (1) | bad | bad | 0.211 (0.160 ... 0.248) | 0.090 (-0.10 ... 0.30) | 55.91 |
| CanESM2 / UCAN_WRF341I CORDEX SAM-44 (1) | reasonable | reasonable | 0.366 (0.285 ... 0.427) | 0.13 (-0.096 ... 0.31) | 43.094 |

5 Multi-method multi-model attribution

This section shows Probability Ratios and change in intensity ΔI for models that passed the validation tests and also includes the values calculated from the fits with observations. All models labelled 'reasonable' have been included, although we note that these models all miss some essential physics.

Table 5: *Precipitation threshold for the 500-yr return period 7-day annual maximum precipitation, Probability Ratio and change in intensity for the models that passed the validation tests, for the study region.*

| Model / Observations | Threshold for return period 500 yr | Probability ratio PR [-] | Change in intensity ΔI [%] |
|--|------------------------------------|---------------------------------|------------------------------------|
| 75 stations | 33.956 mm/day | 4.3e+4 (1.7 ... ∞) | 27 (0.95 ... 59) |
| FLOR historical-rcp45 (5) | 45 mm/day | 1.5 (1.1 ... 2.0) | 3.5 (0.71 ... 6.4) |
| CNRM-CM6-1-HR HighResMIP (1) | 28 mm/day | 0.27 (0.0020 ... 43) | -11 (-23 ... 5.0) |
| EC-Earth3P-HR HighResMIP (1) | 20 mm/day | 0.49 (0.0092 ... 9.8) | -8.5 (-33 ... 25) |
| HadGEM3-GC31-HM HighResMIP (1) | 38 mm/day | 54 (0.089 ... ∞) | 18 (-15 ... 55) |
| HadGEM3-GC31-MM HighResMIP (1) | 45 mm/day | 0.91 (0.057 ... 25) | -1.4 (-28 ... 30) |
| AM2.5C360 AMIP (10) | 48 mm/day | 0.74 (0.18 ... 2.2) | -2.6 (-12 ... 6.4) |
| NorESM1-M / REMO2015 CORDEX SAM-22 (1) | 29 mm/day | 0.15 (0.000077 ... ∞) | -19 (-37 ... 14) |
| MIROC5 / SMHI-RCA4 CORDEX SAM-44 (1) | 59 mm/day | 4.1 (0.19 ... 5.1e+5) | 19 (-10 ... 63) |
| HadGEM2-ES / SMHI-RCA4 CORDEX SAM-44 (1) | 38 mm/day | ∞ (2.5e+2 ... ∞) | 16 (-0.23 ... 35) |

Table 6: Precipitation threshold for the 1000-yr return period 15-day annual maximum precipitation, Probability Ratio and change in intensity for the models that passed the validation tests, for the study region.

| Model / Observations | Threshold for return period 1000 yr | Probability ratio PR [-] | Change in intensity ΔI [%] |
|--|-------------------------------------|---------------------------------|------------------------------------|
| 75 stations | 23.945 mm/day | ∞ (0.12 ... ∞) | 15 (-7.5 ... 47) |
| FLOR historical-rcp45 (5) | 32 mm/day | 1.7 (1.2 ... 3.0) | 3.6 (1.5 ... 6.1) |
| EC-Earth3P-HR HighResMIP (1) | 14 mm/day | 0.57 (0.015 ... 1.7e+3) | -5.0 (-28 ... 26) |
| HadGEM3-GC31-HM HighResMIP (1) | 29 mm/day | 5.4 (0.019 ... ∞) | 7.0 (-15 ... 37) |
| HadGEM3-GC31-MM HighResMIP (1) | 33 mm/day | 0.49 (0.0045 ... 5.6) | -9.3 (-33 ... 17) |
| AM2.5C360 AMIP (10) | 37 mm/day | 0.58 (0.095 ... 2.3) | -4.2 (-15 ... 7.3) |
| NorESM1-M / REMO2015 CORDEX SAM-22 (1) | 19 mm/day | 0.020 (0.0000080 ... ∞) | -23 (-41 ... -0.83) |
| MIROC5 / SMHI-RCA4 CORDEX SAM-44 (1) | 33 mm/day | 42 (0.67 ... ∞) | 18 (-8.6 ... 50) |
| HadGEM2-ES / SMHI-RCA4 CORDEX SAM-44 (1) | 28 mm/day | ∞ (14 ... ∞) | 10 (-4.4 ... 25) |
| NorESM1-M / SMHI-RCA4 CORDEX SAM-44 (1) | 34 mm/day | 0.32 (0.00024 ... ∞) | -9.0 (-35 ... 32) |

6 Hazard synthesis

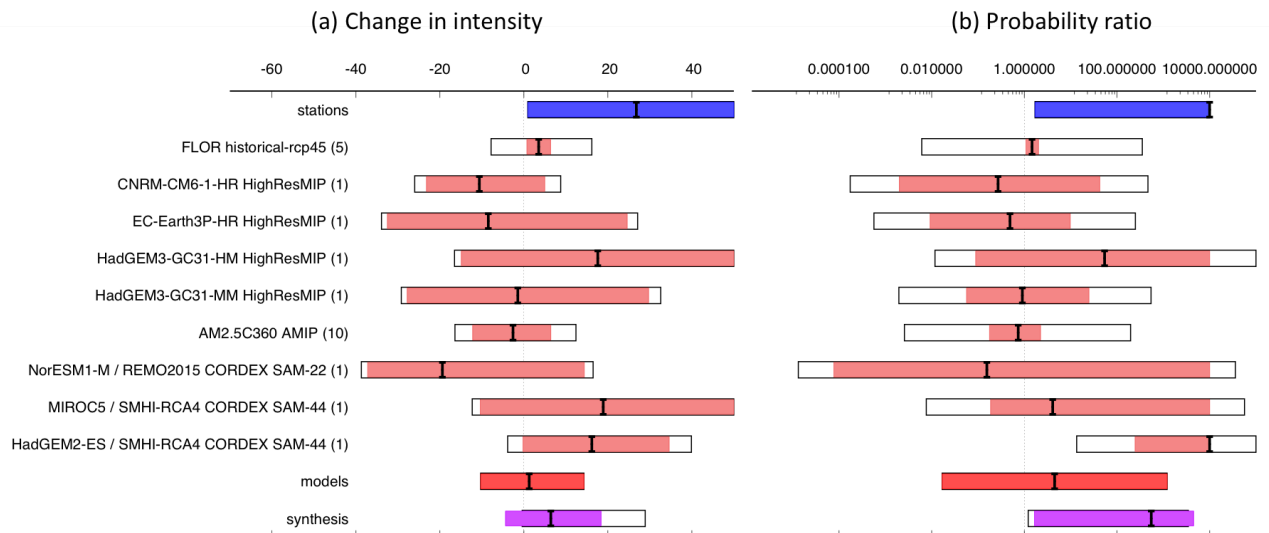


Figure 8: Synthesis of intensity change (left) and probability ratios (right), when comparing the 7-day annual maximum event with a 1.2degC cooler climate.

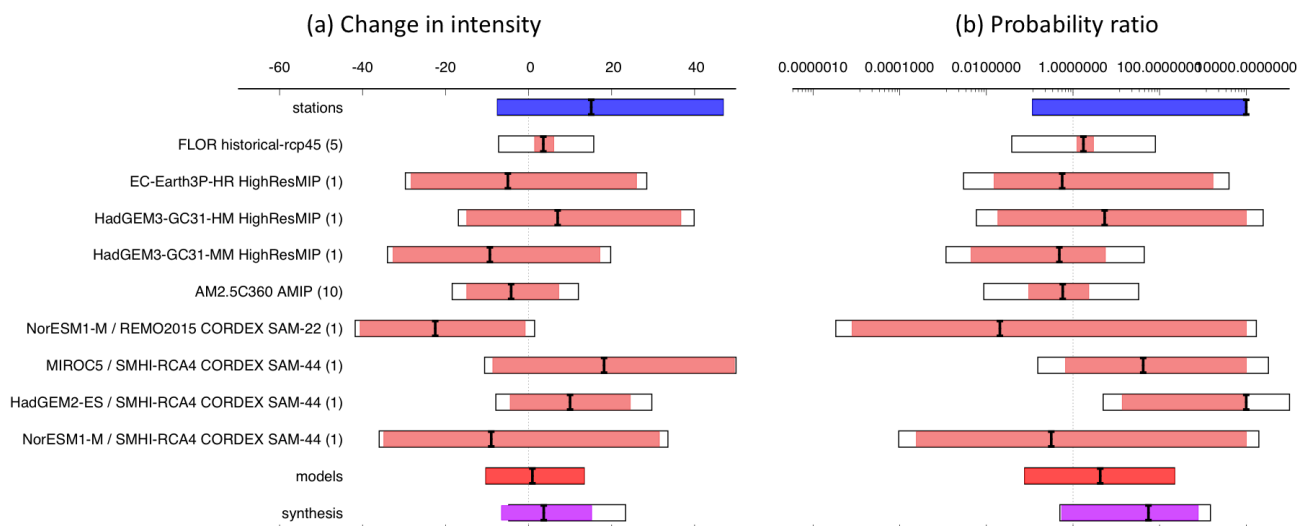


Figure 9: Synthesis of intensity change (left) and probability ratios (right), when comparing the 15-day annual maximum event with a 1.2degC cooler climate.

For both the 7-day annual maximum and the 15-day annual maximum we calculate the probability ratio as well as the change in magnitude of the event in the observations and the models. If the models do not pass the validation tests we do not use the results. We synthesise the ones that pass with the observations to give an overarching attribution statement. Observations and models are combined into a single result in two ways if they seem to be compatible. Firstly, we neglect common model uncertainties beyond the model spread that is depicted by the model average, and compute the weighted average of models and observations: this is indicated by the magenta bar. As, due to common model uncertainties, model uncertainty can be larger than the model spread, secondly, we also show the more conservative estimate of an unweighted average of observations and models, indicated by the white box around the magenta bar in the synthesis figures.

As explained in Section 4, the models are not able to produce the rainfall in May to August, which has a warm convective character. Therefore results of the models that passed our validation tests are considered to be of limited value only. Moreover, the model estimates of changes in intensity and probability do not show a consistent change. Because of these model deficiencies we can not use the synthesised values that combine observations with models. We therefore conclude that observations show a trend towards heavier precipitation on the 7-day and 15-day time scales, although with large uncertainties due to natural variability. We first need to improve the representation of this type of warm rainfall in models before we can present model results with more confidence.

7 Vulnerability and exposure

In addition to assessing the changing risk of the rainfall that contributed to the flood hazard, in this section we look at the vulnerability and exposure factors that increased the likelihood of impacts in the affected region.

Despite Brazil's significant socio-economic progress (e.g. 29 million people lifted out of poverty between 2003-14), inequality, disparities, marginalisation and displacement remain

major drivers of vulnerability ([Kakinuma et al., 2020](#), [Lemos et al., 2016](#); [Dolman et al., 2015](#)), further amplified by climate change impacts ([Debortoli et al., 2017](#); [Rasch, 2015](#)). Vulnerabilities and their implications are unequally distributed across rural/urban divides and ethnicities ([Gubert et al., 2016](#), [Oliveira et al., 2020](#)).

Northeast Brazil is the country's poorest and least developed region ([Hummell, Cutter and Emrich, 2016](#)). It has the lowest average municipality equivalized median monthly household income at R\$429, ([Rasch, 2017](#)). Cities and urban planning can highlight underlying inequities especially for marginalised or disadvantaged ethnic groups and residents of slave-descendant communities ([Gubert et al., 2017](#)).

7.1 History of floods

The Pernambuco and Alagoas states, and in particular their coastal areas, have a long history of flooding. The risk of recurring floods is well-known among affected communities ([Ardaya et al., 2017](#)). For example, floods in 2010 mainly impacted these two states and resulted in entire villages being destroyed, 120,000 people displaced and destruction of roads, bridges, ICT infrastructure and more ([Relief Web, 2010](#)). In Pernambuco, the losses and damages were estimated at R\$ 3,4 billion ([Banco Mundial, 2012a](#)), while in Alagoas resulted in R\$ 1,89 billion ([Banco Mundial, 2012b](#)).

In 2017 another flood in the same states resulted in local states of emergency being declared and over 55,000 people displaced. Between 1995 and 2019, Pernambuco had accumulated losses in disasters that reached R\$ 29,1 billion - the fourth position between the 27 federative units in Brazil - while Alagoas had R\$ 8,9 billion - the 15th position ([Banco Mundial, 2020](#)). The number of housing units destroyed in disasters were 20,300 in Pernambuco (3rd position in the country) and 16,400 in Alagoas (6th position) ([Banco Mundial, 2020](#)). Over the past years, several participatory actions including crowd-sourcing geo-information have been piloted to improve flood risk management ([Mansur et al., 2017](#); [Horita et al., 2015](#); [Degrossi et al., 2014](#)).

7.2 Land-use planning and urbanisation

Situated on the coast of the Atlantic Ocean at the confluence of the Capibaribe and Beberibe rivers and over 70 canals, the Metropolitan Region of Recife (MRR) was amongst the hardest hit by the 2022 flood ([de Souza Leao, Andrade and Nascimento, 2021](#)). Recife, the state capital of Pernambuco, is one of the most at risk cities in Brazil with high population density (7,602 people/km²) and poverty rates (40 percent) paired with significant Black, Brown and Indigenous communities (approximately 59 percent combined) ([Hummell, Cutter and Emrich, 2016](#); [City Population, 2021](#); [Global Future Cities, n.d.](#); [IBGE Census, 2010](#)).

The region has seen rapid urbanisation and increased population density caused by population increases and migration. The broader northeast Brazil region is subject to recurring droughts that have resulted in mass migrations to already overcrowded urban centres ([Marengo et al., 2021](#)). For instance, between 1950 and 2000, the urban population of Recife tripled ([IBGE,](#)

2020) - based on the 2010 National Census, there were 1,5 million people living in the city which has landscape characteristics (low average altitude, flat areas, a water table close to the surface) which make it particularly exposed to hydrometeorological hazards ([de Souza Leao, Andrade and Nascimento, 2021](#)). According to the census, 13.4% of the city's populations lives in high and very high risk-prone areas; 644, 620 in Jaboatão dos Guararapes, 29.2% lived in in landslide or flood-prone areas mapped by the Brazilian Geological Survey ([IBGE, 2018](#)).



Figure 10: Housing inequalities in Recife before the 2022 disaster (Photo: Miguel Angel Trejo Rangel, October 14, 2021)

In line with other regions in Brazil, the urban frontier expands with little oversight and planning, and often results in concentration of informal settlements on flood-prone areas or on/near steep slopes at risk of landslides ([Gomes et al., 2012](#)). Many of the rural migrants live in informal settlements which presently make up nearly one-fourth of the Metropolitan Region of Recife's 3,7 million residents ([Koster, 2020](#)). Falling beyond official municipal boundaries, homes in these informal settlements are often situated on steep hillslopes and along floodplains ([Marengo et al., 2021](#)). The houses built are often shacks made of wood, metal sheets, mud bricks, without a foundation established on firm ground (bedrock). This, coupled with the removal of vegetation, destabilises the soil making it prone to landslides when soaked, a phenomenon documented in several hills in the Recife municipality ([Maia Lins et al., 2020](#)).

The creation of impervious surface and changes to local hydrology and geology has also had an impact on increasing flood and landslide risk, hampering the effectiveness of drainage and sanitation systems, and increasing flood risk ([de Souza Leao et al., 2021](#); [Cerqueira et al.,](#)

[2019](#)). Urban sanitation and drainage infrastructure is inadequate, usually due to a lack of planning and assessments deemed incompatible to current needs of most cities around the country ([Rodrigues et al., 2022](#)).

7.3 Risk management - preparedness, early warning early action, and response

Planning and preparedness play a key role in reducing the vulnerability and exposure of people and assets during disasters.

In Brazil, different flood risk management laws and policies exist at national, provincial, and municipal scale. For instance, 1,538 (27.6%) of 5,570 municipalities have urban plans which take into account flood risks ([IBGE, 2020](#)) - in the Northeast region, 18.7% of municipalities have these plans. Brazil's National Center for Monitoring and Early Warning of Natural Disasters (CEMADEN) was created in July 2011, after the devastating Petropolis floods and landslides ([Marchezini et al. 2017](#)). Sitting at the Ministry of Science, Technology and Innovation. CEMADN currently monitors 1038 cities in Brazil - with landslide and flood maps which were developed by the Brazilian Geological Survey (CPRM, 2022) - and is responsible for issuing alerts to the National Secretariat of Civil Defense (SEDEC).

The State of Pernambuco's Water and Climate Agency (APAC) also has a flood early warning system by which alerts are issued to the public. The warnings range from yellow to orange to red, the combination of probability of occurrence and the intensity of the rain events (APAC 2022). APAC also participates in the training of Municipal Civil Defences, explaining how the weather forecasts work and the three types of alerts (yellow, orange and red), based on the daily weather forecasting and tendencies updates. All representatives of the municipal Civil Defences have direct communication with the APAC Situation Room, and from these updates and trainings, each municipality is responsible for updating its disaster risk reduction (DRR) and contingency plan annually - 24.3% of cities have DRR plans in Pernambuco ([IBGE, 2020](#)). In addition to media outlets, policies enacted in response to previous flood events enabled the alerts to be issued through SMS, although the text of a current bill under consideration by the Recife Assembly suggests these SMS warnings are "unavailable", justifying the introduction of this additional bill to strengthen Recife's response programs ([Bill 32/2022 April 2022](#)). Finally, each municipality is responsible for developing procedures for preventive measures in case of disasters. Every year, the members of the Municipal Civil Defences are trained to update such measures for the rainy season in the State of Pernambuco.

For this event, the severe rainfall that contributed to the floods and landslides was relatively well-forecasted albeit with a wide range, with sources such as GLOFAS forecasting flooding between a 2–5-year average to over a 20 year average ([Start Network, May 27, 2022](#); [ECHO, May 31 2022](#)). Conditions were monitored by agencies such as APAC (internal communication) and warning alerts were issued - notably, the municipal government of Recife issued a red alert for heavy rains on May 27. Technical meetings were held between APAC and Pernambuco Civil Defense to support prevention actions based on weather and climate conditions. Federal, State and Municipal disaster response included search and rescue, first aid provision, and the restoration of essential services all which would have reduced the impacts of the events once they had occurred ([Ministério do Desenvolvimento Regional, 2022](#)). Pernambuco State Government has announced to also provide financial support for disaster

recovery to the affected population ([Bill 17810 June 2022](#)).

Recent research also points to potential policy implementation gaps that may need improvement to increase the effectiveness of climate and disaster risk reduction policies and structures. Political action has historically followed on the heels of large disasters and this reactive approach to the challenges has not (yet) led to a complete integration of all levels and links in the warning systems chain. This is a politically charged subject made more complex in times of political instability and economic recession ([Marchezini et al. 2017](#)). If left unresolved, this situation may contribute to increasing vulnerability and risks of disasters.

7.4 Conclusions

The rainfall that resulted in flash floods in coastal northeastern Brazil was very rare (a 1-500 to 1-1000 year event), and we can reasonably assume that such a rare event will be an impactful one. The extreme nature of the floods made it so that exposure was the main determinant of impact, although long-term impacts and recovery will likely be mediated by socio-economic, demographic and governance factors. An increase in urbanisation, especially unplanned and informal in low-lying flood-prone areas and steep hillsides have increased the community exposure to these hazards. The need for improving the linkage between early warning and prevention actions is highlighted. It is unclear to what extent the warning helped reduce the impacts, even though some actions were taken by Civil Defense. However it was not possible to prevent fatalities because of the magnitude of the extreme rainfall events. This indicates the need to review and strengthen the linkage between weather warnings and the process that would lead to improved anticipatory action based on those warnings. This region also generally has an infrastructure deficit (e.g. housing, roads, water and sanitation etc.). As new infrastructure is built, there is an opportunity to increase resilience by accounting for increasing risks in the design and location, instead of reverting to outdated design standards.

Data availability

Almost all data are or will soon be available via the Climate Explorer. For access to weather station data please contact the National Institute of Meteorology (INMET) and National Water and Sanitation Agency (ANA).

References

- Alvares, C.A., Stape, J.L. Sentelhas, P.C., de Moraes, G.g Leonardo, J. & Sparovek, G. (2013). Koppen's Climate classification maps for Brazil. *Meteorologische Zeitschrift*, 22(6), 711-728. <https://doi.org/10.1127/0941-2948/2013/0507>
- Andreoli, R. V., & Kayano, M. T. (2007). A importância relativa do atlântico tropical sul e pacífico leste na variabilidade de precipitação do Nordeste do Brasil. *Revista*

- Chan, D., Vecchi, G. A., Yang, W., and Huybers, P. (2021). Improved simulation of 19th-and 20th-century North Atlantic hurricane frequency after correcting historical sea surface temperatures. *Sci. Adv.* 7, eabg6931. <https://doi.org/10.1126/sciadv.abg6931>
- Ciavarella, A., Cotterill, D., Stott, P., Kew, S., Philip, S., van Oldenborgh, G. J., et al. (2021). Prolonged Siberian heat of 2020 almost impossible without human influence. *Climatic Change*, 166 (1), 9. <https://doi.org/10.1007/s10584-021-03052-w>
- Civil Defense- *Alagoas* (2022). Personal communication on 27 June 2022. Maceió.
- Civil Defense- *Pernambuco* (2022). By Secretary of Pernambuco. Daily report on 27 June 2022. Recife.
- Costa, M. B. S. F., Mallmann, D. L., Pontes, P. M., & Araujo, M. (2010). Vulnerability and impacts related to the rising sea level in the Metropolitan Center of Recife, Northeast Brazil. *Pan-American Journal of Aquatic Sciences*, 5(2), 341-349. Retrieved from [https://panamjas.org/pdf_artigos/PANAMJAS_5\(2\)_341-349.pdf](https://panamjas.org/pdf_artigos/PANAMJAS_5(2)_341-349.pdf)
- Debortoli, N. S., Camarinha, P. I. M., Marengo, J. A., & Rodrigues, R. R. (2017). An index of Brazil's vulnerability to expected increases in natural flash flooding and landslide disasters in the context of climate change. *Natural Hazards*, 86(2), 557–582. <https://doi.org/10.1007/s11069-016-2705-2>
- Delworth, T. L., Rosati, A., Anderson, W., Adcroft, A. J., Balaji, V., Benson, R., Dixon, K., Griffies, S. M., Lee, H.-C., Pacanowski, R. C., Vecchi, G. A., Wittenberg, A. T., Zeng, F., and Zhang, R. (2012). Simulated Climate and Climate Change in the GFDL CM2.5 High-Resolution Coupled Climate Model. *J. Clim.* 25, 2755–2781. <https://doi.org/10.1175/JCLI-D-11-00316.1>.
- Giorgi, F., Coppola, E., Teichmann, C., and Jacob, D. (2021). Editorial for the CORDEX-CORE experiment I special issue. *Clim. Dyn.* 57, 1265–1268. <https://doi.org/10.1007/s00382-021-05902-w>
- Gomes, H. B., Ambrizzi, T., Herdies, D. L., Hodges, K., & Pontes da Silva, B. F. (2015). Easterly Wave Disturbances over Northeast Brazil: An Observational Analysis. *Advances in Meteorology*, 2015, 1–20. <https://doi.org/10.1155/2015/176238>
- Gutowski, W. J., Giorgi, F., Timbal, B., Frigon, A., Jacob, D., Kang, H.-S., Raghavan, K., Lee, B., Lennard, C., Nikulin, G., O'Rourke, E., Rixen, M., Solman, S., Stephenson, T., and Tangang, F. (2016). WCRP COordinated Regional Downscaling EXperiment (CORDEX): a diagnostic MIP for CMIP6. *Geosci. Model Dev.* 9, 4087–4095. <https://doi.org/10.5194/gmd-9-4087-2016>.
- Haarsma, R. J., Roberts, M. J., Vidale, P. L., Senior, C. A., Bellucci, A., Bao, Q., Chang, P., Corti, S., Fučkar, N. S., Guemas, V., von Hardenberg, J., Hazeleger, W., Kodama, C., Koenigk, T., Leung, L. R., Lu, J., Luo, J.-J., Mao, J., Mizielinski, M. S., Mizuta,

- R., Nobre, P., Satoh, M., Scoccimarro, E., Semmler, T., Small, J., and von Storch, J.-S. (2016). High Resolution Model Intercomparison Project (HighResMIP v1.0) for CMIP6. *Geosci. Model Dev.* 9, 4185–4208. <https://doi.org/10.5194/gmd-9-4185-2016>
- Hansen, J., Ruedy, R., Sato, M., & Lo, K. (2010). Global surface temperature change. *Reviews of Geophysics*, 48(4). <https://doi.org/10.1029/2010RG000345>
- Hersbach, H., Bell, B., Berrisford, P., Hirahara, S., Horányi, A., Muñoz-Sabater, J., ... & Thépaut, J. N. (2020). The ERA5 global reanalysis. *Quarterly Journal of the Royal Meteorological Society*, 146(730), 1999-2049. <https://doi.org/10.1002/qj.3803>
- Huang, B., Thorne, P. W., Banzon, V. F., Boyer, T., Chepurin, G., Lawrimore, J. H., Menne, M. J., Smith, T. M., Vose, R. S., & Zhang, H. (2017). Extended Reconstructed Sea Surface Temperature, Version 5 (ERSSTv5): Upgrades, Validations, and Intercomparisons, *Journal of Climate*, 30(20), 8179-8205. <https://journals.ametsoc.org/view/journals/clim/30/20/jcli-d-16-0836.1.xml>
- Jones, N. (2022). Rare'triple'La Niña climate event looks likely-what does the future hold?. *Nature*. <https://doi.org/10.1038/d41586-022-01668-1>
- Kouadio, Y. K., Servain, J., Machado, L. A. T., & Lentini, C. A. D. (2012). Heavy Rainfall Episodes in the Eastern Northeast Brazil Linked to Large-Scale Ocean-Atmosphere Conditions in the Tropical Atlantic. *Advances in Meteorology*, 2012, 1–16. <https://doi.org/10.1155/2012/369567>
- Lenssen, N., Schmidt, G., Hansen, J., Menne, M., Persin, A., Ruedy, R., and Zyss, D. (2019). Improvements in the GISTEMP uncertainty model. *J. Geophys. Res. Atmos.*, 124(12), 6307-6326, <https://doi.org/10.1029/2018JD029522>.
- Liu, C., & Zipser, E. J. (2009). “Warm Rain” in the Tropics: Seasonal and Regional Distributions Based on 9 yr of TRMM Data, *Journal of Climate*, 22(3), 767-779. <https://doi.org/10.1175/2008JCLI2641.1>
- Philip, S., Kew, S., van Oldenborgh, G. J., Otto, F., Vautard, R., van der Wiel, K., et al. (2020). A protocol for probabilistic extreme event attribution analyses. *Adv. Stat. Clim. Meteorol. Oceanogr.*, 6, 177–203, <https://doi.org/10.5194/ascmo-6-177-2020>, 2020.
- Rayner, N. A. A., Parker, D. E., Horton, E. B., Folland, C. K., Alexander, L. V., Rowell, D. P., ... & Kaplan, A. (2003). Global analyses of sea surface temperature, sea ice, and night marine air temperature since the late nineteenth century. *Journal of Geophysical Research: Atmospheres*, 108(D14). <https://doi.org/10.1029/2002JD002670>
- Ramos, R. P. L. (1975). Precipitation characteristics in the Northeast Brazil dry region. *Journal of Geophysical Research*, 80(12), 1665-1678. <https://doi.org/10.1029/JC080i012p01665>

- Rodrigues, D. T., Gonçalves, W. A., Spyrides, M. H. C., Santos e Silva, C. M., & de Souza, D. O. (2020). Spatial distribution of the level of return of extreme precipitation events in Northeast Brazil. *International Journal of Climatology*, 40(12), 5098–5113. <https://doi.org/10.1002/joc.6507>
- Rozante, J. R.; Moreira, D. S. ; Gonçalves., L. G. G. & Vila, D.A. (2010). Combining TRMM and Surface Observations of Precipitation: Technique and Validation Over South America. *Weather and Forecasting*, v. 25, p. 885-894. <https://doi.org/10.1175/2010WAF2222325.1>
- Rudorff, C., Sparrow, S., Guedes, M.R.G., Tett, S.F.B., Brêda, J.P.L.F., Cunningham, C., Ribeiro, F.N.D., Palharini, R.S.A. & Lott, F.C. (2021) Event attribution of Parnaíba River floods in Northeastern Brazil. *Climate Resil Sustain*, 1, e16. <https://doi.org/10.1002/cli2.16>
- Schneider, Udo; Becker, Andreas; Finger, Peter; Rustemeier Elke; Ziese, Markus (2020): GPCP Monitoring Product: Near Real-Time Monthly Land-Surface Precipitation from Rain-Gauges based on SYNOP and CLIMAT data. DOI: 10.5676/DWD_GPCP/MP_M_V2020_100; http://dx.doi.org/10.5676/DWD_GPCP/MP_M_V2020_100
- Silva, T. L. do V., & de Souza Guedes, R. V. (2012). Análise do Comportamento Atmosférico em Situação de Seca: Uma Abordagem Operacional para Pernambuco (Analysis of Atmospheric Behavior Under Drought Condition: An Operational Approach to Pernambuco). *Revista Brasileira de Geografia Física*, 5(4), 937-950. Retrieved from <https://periodicos.ufpe.br/revistas/rbgfe/article/download/232880/26871>
- Silva, T. L. do V., Veleda, D., Araujo, M., & Tyaquiçã, P. (2018). Ocean-atmosphere feedback during extreme rainfall events in eastern Northeast Brazil. *Journal of Applied Meteorology and Climatology*, 57(5), 1211–1229. <https://doi.org/10.1175/JAMC-D-17-0232.1>
- Taylor, K. E., Stouffer, R. J., & Meehl, G. A. (2012). An overview of CMIP5 and the experiment design. *Bulletin of the American meteorological Society*, 93(4), 485-498. <https://doi.org/10.1175/BAMS-D-11-00094.1>.
- Torres, R. R., & Ferreira, N. J. (2011). Case Studies of Easterly Wave Disturbances over Northeast Brazil Using the Eta Model. *Weather and Forecasting*, 26(2), 225–235. <https://doi.org/10.1175/2010WAF2222425.1>
- van Oldenborgh, G. J., van der Wiel, K., Kew, S., Philip, S., Otto, F., Vautard, R., et al. (2021). Pathways and pitfalls in extreme event attribution. *Climatic Change*, 166 (1), 13. <https://doi.org/10.1007/s10584-021-03071-7>
- Vecchi, G. A., Delworth, T., Gudgel, R., Kapnick, S., Rosati, A., Wittenberg, A. T., ... & Zhang, S. (2014). On the seasonal forecasting of regional tropical cyclone activity. *Journal of Climate*, 27(21), 7994-8016. <https://doi.org/10.1175/JCLI-D-14-00158.1>

Waliser, D. E., and X. Jiang, 2015: Tropical meteorology: Intertropical convergence zone. Encyclopedia of Atmospheric Sciences, 2nd ed. G. R. North, J. Pyle, and F. Zhang, Eds., Elsevier, 121–131.

Yang, W., Hsieh, T. L., & Vecchi, G. A. (2021). Hurricane annual cycle controlled by both seeds and genesis probability. *Proceedings of the National Academy of Sciences*, 118(41), e2108397118. <https://doi.org/10.1073/pnas.2108397118>

Ziese, Markus; Becker, Andreas; Finger, Peter; Meyer-Christoffer, Anja; Rudolf, Bruno; Schneider, Udo (2011): GPCP First Guess Product at 1.0°: Near Real-Time First Guess monthly Land-Surface Precipitation from Rain-Gauges based on SYNOP Data. https://doi.org/10.5676/DWD_GPCP/FG_M_100.

Supplementary Material

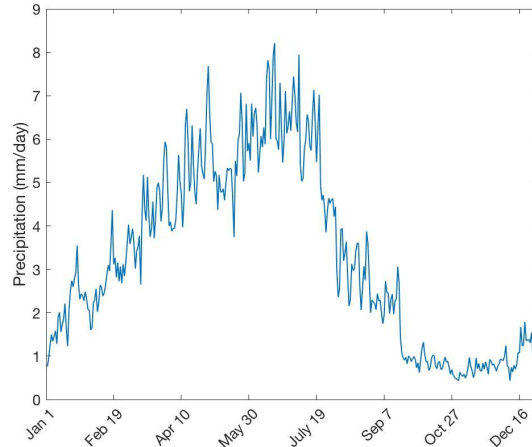


Figure S1: Seasonal cycle of precipitation from station data over the study area, based on station data. The seasonal cycle was determined from data for the years 1960 to 2022

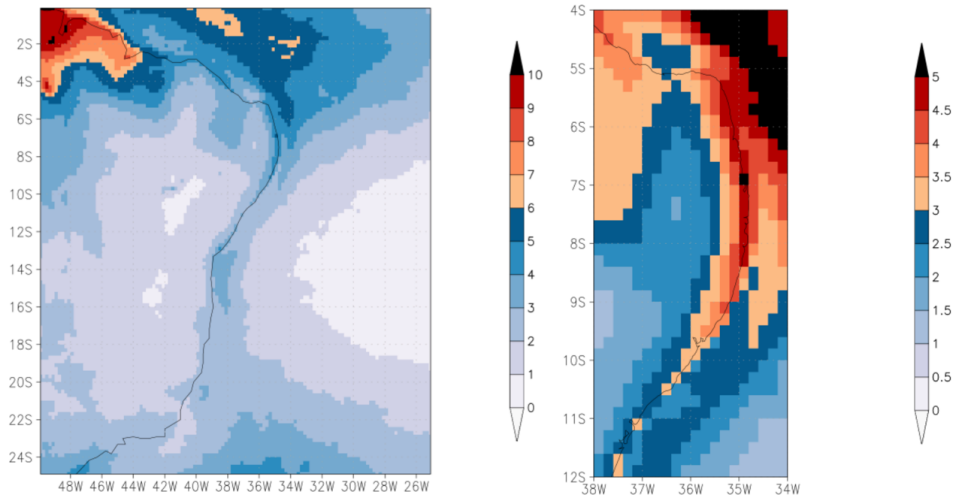
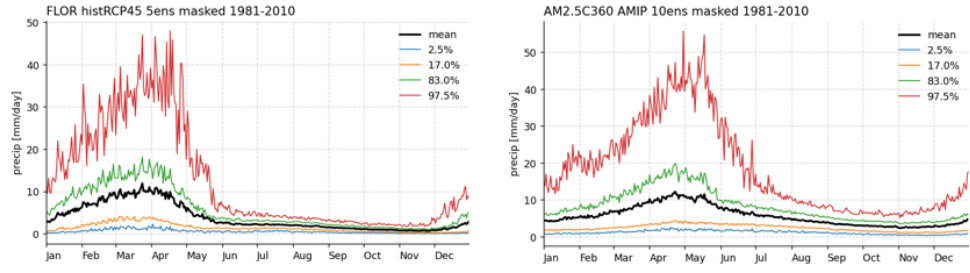
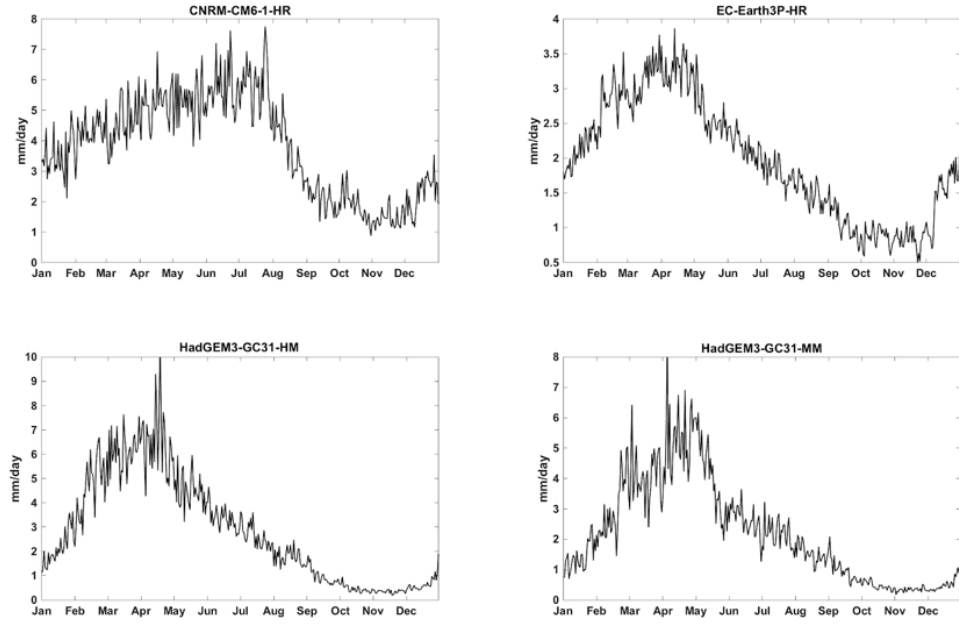


Figure S2: Spatial pattern of average rainfall over March-Aug, based on GPM-IMERG dataset. The spatial pattern was calculated from data over 2001-2022

(a) GFDL models



(b) HighResMIP models



(c) CORDEX models

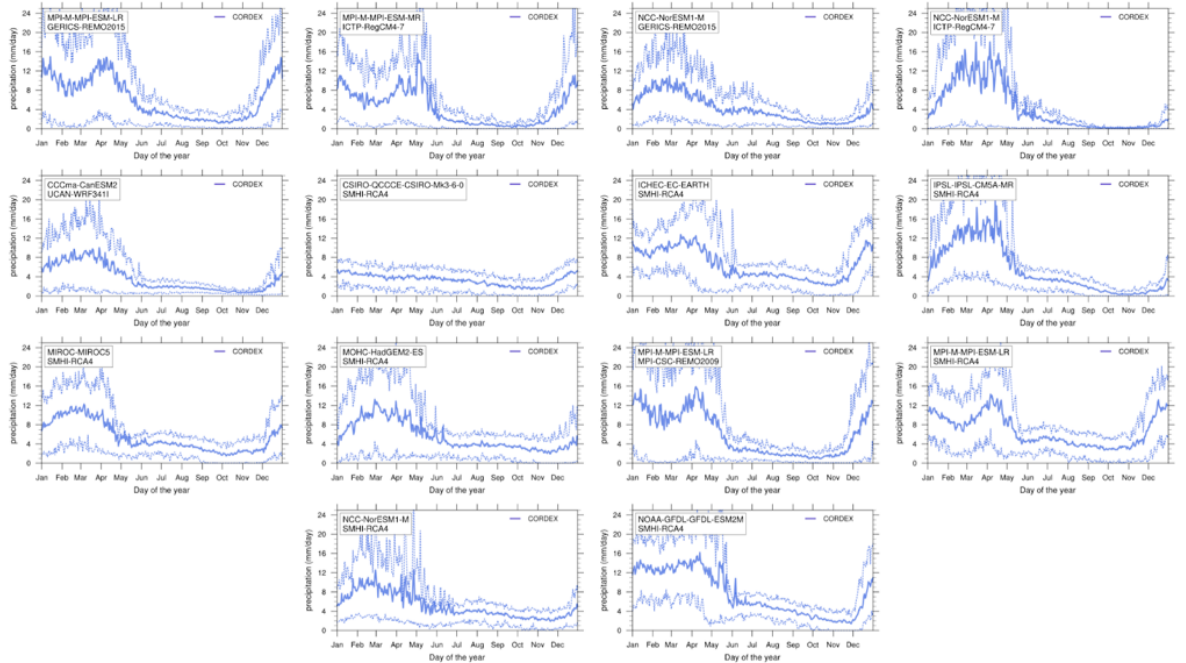
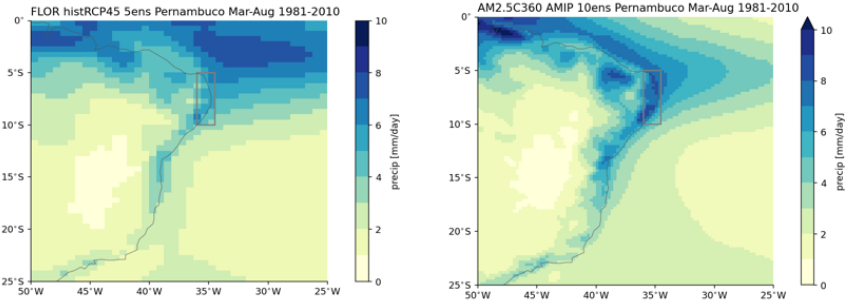
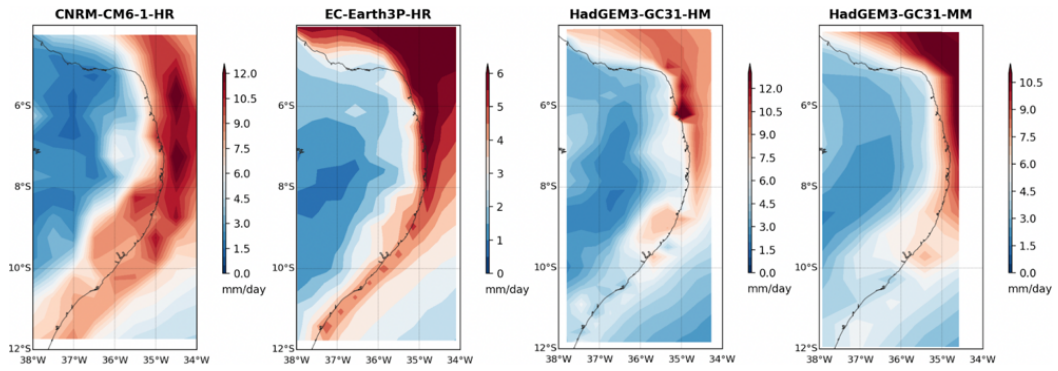


Figure S3: Seasonal cycle of precipitation from over the study area from (a) GFDL models (b) HighResMIP models and (c) CORDEX models

(a) GFDL models



(b) HighResMIP models



(c) CORDEX models

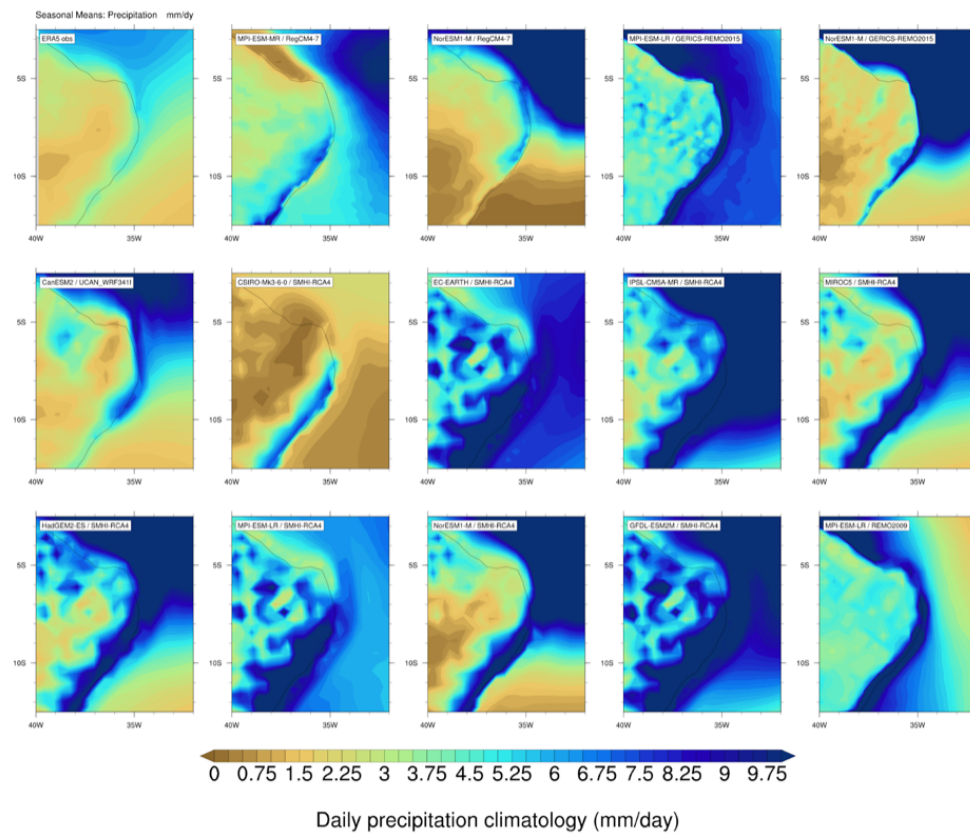


Figure S4: Spatial pattern of average rainfall over March-Aug, from (a) GFDL models (b) HighResMIP models and CORDEX models

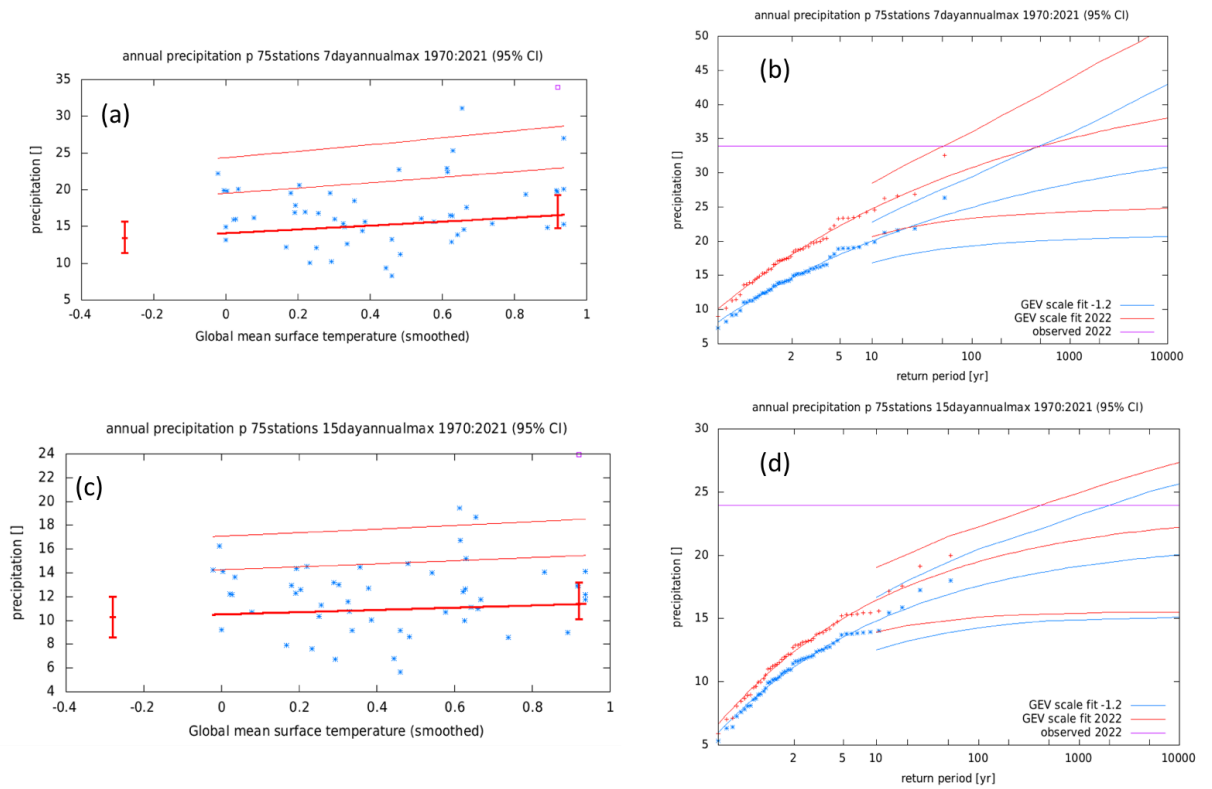


Figure S5: (a) GEV fit with constant dispersion parameter, and location parameter scaling proportional to GMST, for the average over 75 stations from 1970-2022. No information from 2022 is included in the fit. **Left:** Annual 7-day (a) and 15-day (c) average rainfall as a function of the smoothed GMST. The thick red line denotes the time-varying location parameter. The vertical red lines show the 95% confidence interval for the location parameter, for the current, 2022 climate and the fictional, 1.2°C cooler climate. The 2022 observation is highlighted with the magenta box. **Right:** Return time plots for the climate of 2022 (red) and a climate with GMST 1.2°C cooler (blue), for the 7-day average (b) and the 15-day average (d). The past observations are shown twice: once shifted up to the current climate and once shifted down to the climate of the late nineteenth century. The markers show the data and the lines show the fits and uncertainty from the bootstrap. The magenta line shows the magnitude of the 2022 event analysed here.

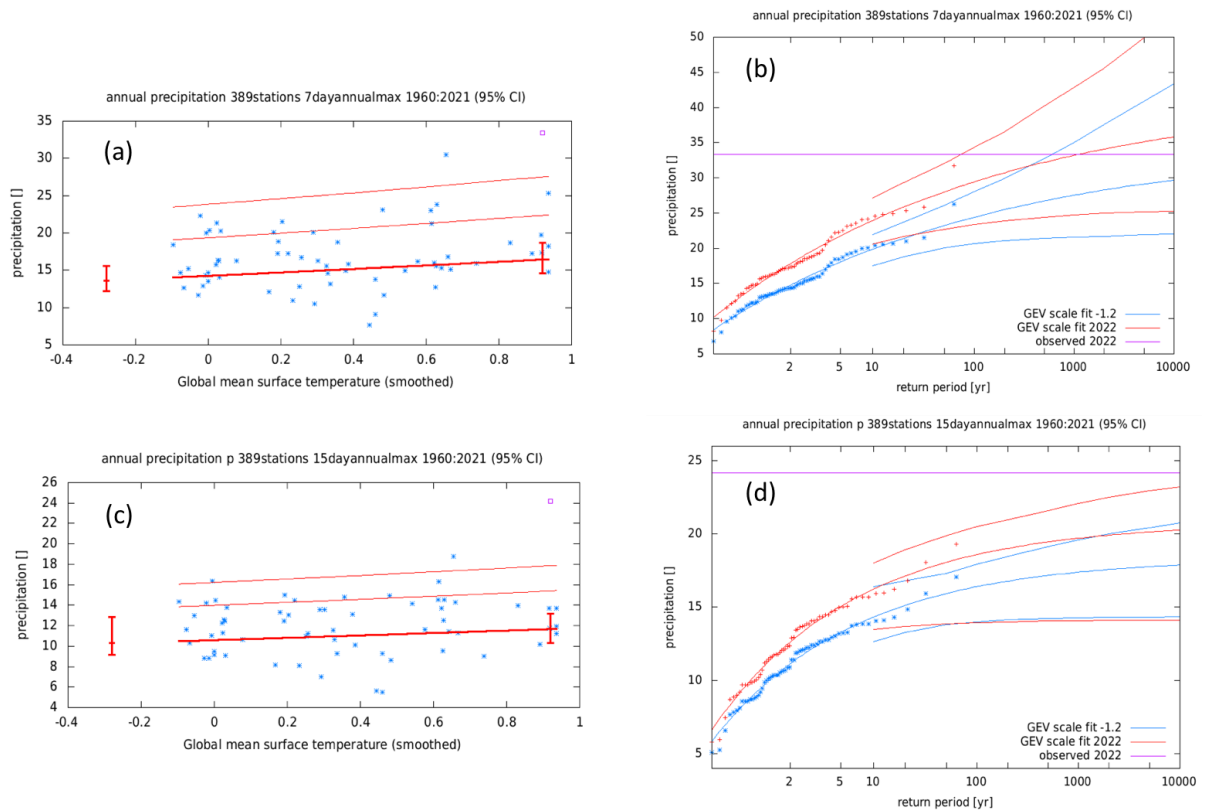


Figure S6: (a) GEV fit with constant dispersion parameter, and location parameter scaling proportional to GMST, for the average over all 389 stations from 1960-2022. No information from 2022 is included in the fit. **Left:** Annual 7-day (a) and 15-day (c) average rainfall as a function of the smoothed GMST. The thick red line denotes the time-varying location parameter. The vertical red lines show the 95% confidence interval for the location parameter, for the current, 2022 climate and the fictional, 1.2°C cooler climate. The 2022 observation is highlighted with the magenta box. **Right:** Return time plots for the climate of 2022 (red) and a climate with GMST 1.2°C cooler (blue), for the 7-day average (b) and the 15-day average (d). The past observations are shown twice: once shifted up to the current climate and once shifted down to the climate of the late nineteenth century. The markers show the data and the lines show the fits and uncertainty from the bootstrap. The magenta line shows the magnitude of the 2022 event analysed here.